Cell Reports
Physical Science

Article

Role of solvent in the spontaneous resolution of amino acids via formation of supramolecular helices

Graphical abstract

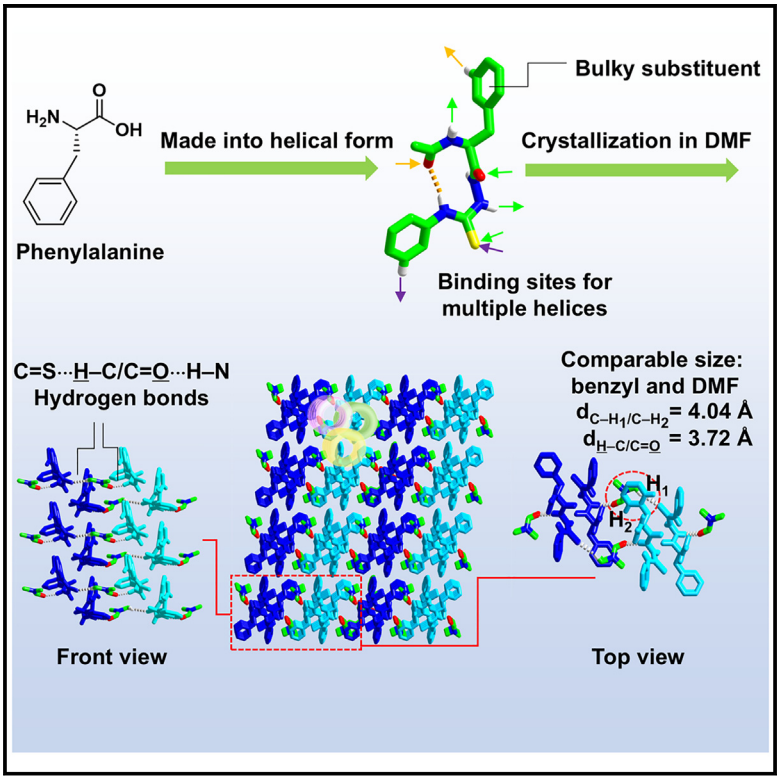

Authors

Peimin Weng, Xiang Lin, Yi-Lin Cai, Xiaosheng Yan, Jinlian Cao, Zhao Li, Yun-Bao Jiang

Correspondence

xshyan@xmu.edu.cn (X.Y.),
ybjiang@xmu.edu.cn (Y.-B.J.)

In brief

Weng et al. report that a helical structural framework with sufficient binding sites for multiple helices derived from phenylalanine undergoes spontaneous resolution owing to the fact that the hydrogen-bonding solvent DMF has a distance comparable to the size of the bulky substituent, enabling it to bridge two neighboring homochiral helices.

Highlights

- Phenylalanine is made into a helical structure with binding sites for multiple helices
- Bulky phenylalanine residue leads to large distance between the formed neighboring helices
- Distance of H-bonding donor and acceptor in DMF is comparable to the size of phenylalanine residue
- DMF H-bonded two neighboring helices of the same helicity to facilitate spontaneous resolution

Weng et al., 2025, Cell Reports Physical Science 6, 102521
April 16, 2025
https://doi.org/10.1016/j.xcrp.2025.102521

CellPress

Cell Reports
Physical Science

CellPress
OPEN ACCESS

Article

Role of solvent in the spontaneous resolution of amino acids via formation of supramolecular helices

Peimin Weng,[1] Xiang Lin,[1] Yi-Lin Cai,[1] Xiaosheng Yan,[1,2,*] Jinlian Cao,[1] Zhao Li,[1] and Yun-Bao Jiang[1,3,*]
[1]Department of Chemistry, College of Chemistry and Chemical Engineering and the MOE Key Laboratory of Spectrochemical Analysis and Instrumentation, Xiamen University, Xiamen 361005, China
[2]Fujian Provincial Key Laboratory of Innovative Drug Target Research and State Key Laboratory of Cellular Stress Biology, School of Pharmaceutical Sciences, Xiamen University, Xiamen 361102, China
[3]Lead contact
*Correspondence: xshyan@xmu.edu.cn (X.Y.), ybjiang@xmu.edu.cn (Y.-B.J.)
https://doi.org/10.1016/j.xcrp.2025.102521

SUMMARY

Spontaneous resolution remains a great challenge. Despite efforts that have been made to design chiral species that can be structurally modified to allow spontaneous resolution, the role of the solvent in which the crystallization is performed has not been extensively explored. We report here the role of the solvent dimethyl formamide (DMF) in the spontaneous resolution of an aromatic amino acid, phenylalanine (F), which contains a bulky benzyl substituent, made in its helical derivatives acetylphenylalanine *N*-amido-*N*′-phenylthiourea (AcFH) and *N*′-(*p*-iodo)phenylthiourea (AcFI). Spontaneous resolution is achieved in DMF or 1:1:1 (v/v/v) DMF/CH_3CN/CH_3OH from which the crystals contain only DMF molecules. This is shown to result from bridging the formed neighboring supramolecular helices of the same helicity by DMF, a hydrogen-bonding solvent containing both the hydrogen-bonding donor and acceptor that are separated by a distance comparable to the size of the substituent in the amino acid residue.

INTRODUCTION

Spontaneous resolution remains a significant challenge. Up to now, fewer than 10% of the racemates crystallize in conglomerates, largely because the mechanisms are elusive,[1–10] and the way of the target chiral compound to be derived, if needed, is not straightforward. We recently proposed a strategy for spontaneous resolution by forming multiple helices to ensure a three-dimensional (3D) homochirality in the crystals[11] and succeeded in the spontaneous resolution of the simplest amino acid, alanine (A), by extracting it into a helical building block, acetylalanine *N*-amido-*N*′-(*p*-X-phenyl)thioureas (**AcAX**, X = I, Br, Cl; Scheme 1), which forms two orthogonal supramolecular helices in two dimensions via intermolecular hydrogen bonding and halogen bonding.[12] This establishes a structural scheme for the chiral compound to be made into a helical building block bearing suitable intermolecular interaction sites.[13]

The choice of the solvent in which crystallization takes place is the other important,[14–21] and even harder to clarify, issue that governs the occurrence of spontaneous resolution, in which several parameters such as intermolecular interactions,[22] solvent polarity,[23] and hydrophilic effect[24] may function, which adds difficulty to the optimization of the structure of the chiral species. In our previous successful cases, no solvent molecules were found within the lattices of the crystals of **AcAX**[12]; therefore, the role of solvent could not be examined. We assume that the small size of the substituent in the alanine residue, $-CH_3$, could be a reason that the distance between the formed helices is too small to accommodate solvent molecules. We thus envisage that following our structural framework, the helical derivatives of an amino acid bearing a bulky substituent that undergoes spontaneous resolution would allow the role of solvent to be elucidated.

We decided to examine the spontaneous resolution of phenylalanine (F), an aromatic amino acid with a bulky benzyl substituent, $-CH_2Ph$, despite the challenges that this aromatic substituent may provide additional intermolecular interaction sites from its aromatic C–Hs and/or phenyl π-ring. It may also impose challenges led by phenyl/phenyl stacking, occurring between two phenylalanine residues, preferably of opposite chirality.[25] Phenylalanine was made into helical L-/D-**AcFI** containing a halogen-bonding I atom and L-/D-**AcFH** without such halogen-bonding atoms in the hope that the other interaction sites in the phenylalanine residue would assist in the intermolecular interactions (Scheme 1). Crystallization was carried out in hydrogen-bonding solvents such as dimethyl formamide (DMF), CH_3CN, and CH_3OH, all containing both hydrogen-bonding donor and acceptor but separated by different distances. Spontaneous resolution was successful in DMF or DMF containing the solvent mixture 1:1:1 (v/v/v) DMF/CH_3CN/CH_3OH. Surprisingly, in the crystals grown in the latter solvent mixture, only DMF molecules were found, and therefore a critical role of the solvent DMF is shown.

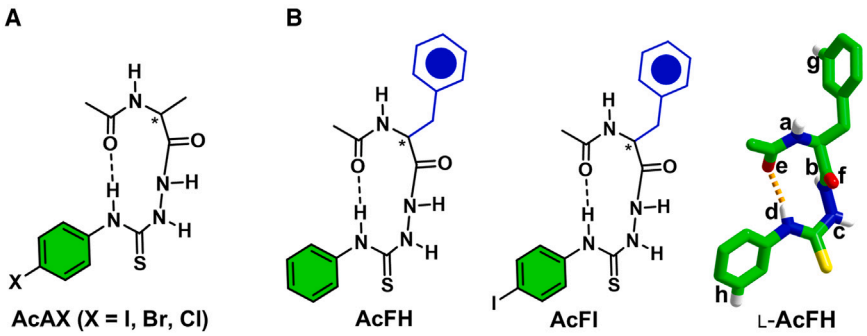

Scheme 1. Molecular design

Structures of (A) **AcAX** (X = I, Br, Cl)[12] and (B) **AcFI** and **AcFH**, including crystal structure of L-**AcFH** with atom labeling. Dashed lines highlight hydrogen bonds that maintain the β-turn structure.

RESULTS

Choice of solvents

AcFI and **AcFH**, like their alanine counterpart **AcAX** (Scheme 1),[12] are short azapeptides rich in hydrogen-bonding sites.[26–29] We thus considered choosing hydrogen-bonding solvents with both hydrogen-bonding donor and acceptor, such as DMF, CH_3CN, and CH_3OH. A quick screening of ^{1}H-NMR spectra of L-**AcFH** in those deuterated solvents revealed well-resolved ^{1}H-NMR signals (Figure 1A), suggesting clear proton environments and the absence of significant aggregation. However, based on the order of the anisotropic factors (*g*) of the crystals of L-**AcFH** grown in those solvents (Figure 1B), we concluded that DMF and CH_3CN facilitate the formation of more organized structures with L-**AcFH**, and therefore would be a better choice to promote spontaneous resolution, if any. The *g* factors of D-**AcFH** crystals grown in different solvents are mirror images of those corresponding to the L-**AcFH** crystals (Figure S1).

This is understandable, since the bulky benzyl substituent in phenylalanine residue may result in a large distance between the formed neighboring helices. A bulky and dipolar hydrogen-bonding solvent would thus be preferred to bridge the neighboring two helices by using its hydrogen bonding donor and acceptor, preferably separated by a distance around a phenyl four carbons in the substituent. For example, DMF (H-CH_2-N(CH_3)-CH = O, 4.15 Å of H···O distance), is superior to CH_3CN (H-CH_2-C≡N, 3.06 Å of H···N distance) and CH_3OH (H-CH_2-O-H, 2.00 Å of H···O distance; Figure S2) of smaller sizes, in which potential hydrogen-bonding donor and acceptor are underlined and their distances are shown.

Growing crystals of enantiomers and racemates of **AcFH** in DMF, CH_3CN, or CH_3OH via slow evaporation at room temperature (25°C) does show that *rac*-**AcFH** crystallizes as a conglomerate in DMF, but not in CH_3CN or CH_3OH; in CH_3CN or CH_3OH, it crystallizes as racemic compounds (for crystallographic data, see Tables S1–S6). It is significant to note that spontaneous resolution takes place with **AcFH**, with no intermolecular halogen-bonding interaction necessary for the resolution of the alanine derivative **AcAI**.[12] There are other driving forces, likely the role of solvent DMF, that promote the resolution of **AcFH**. This observation also implies that the solvent molecule CH_3CN or CH_3OH might be too small to bridge **AcFH** molecules in the neighboring two helices. Very significantly, when crystallization of *rac*-**AcFH** was carried out in 1:1:1 (v/v/v) CH_3CN/CH_3OH/DMF mixed solvent, conglomerate crystals were also obtained, and only DMF molecules were found in the crystals (Table S5), suggesting the critical role of DMF molecules in driving the spontaneous resolution.

In agreement with these observations, the X-ray powder diffraction (XRPD) pattern of the crystals of *rac*-**AcFH** grown in DMF is identical to that of the crystal of enantiopure L-**AcFH** (Figure 2A), whereas the XRPD patterns of crystals of *rac*-**AcFH** grown in CH_3CN or CH_3OH differ from that of the enantiopure L-**AcFH** (Figures 2B and 2C). Circular dichroism (CD) spectra of the crystals grown from *rac*-**AcFH** in DMF are either that of L- or D-**AcFH** (Figure 2D), whereas the CD spectra of crystals grown in CH_3CN or CH_3OH exhibit practically no signals, confirming their racemate nature (Figures 2E and 2F). High-performance liquid chromatography (HPLC) traces of the selected single crystals of *rac*-**AcFH** correspond to either L- or D-**AcFH**, when they are grown in DMF, whereas they exhibit two peaks of the same equivalent when grown in CH_3CN or CH_3OH (Figures 2G–2I). Indeed, X-ray crystal structure analyses show that among five crystals taken in one pot from those grown in DMF, three are of enantiopure L-**AcFH** and two are of D-**AcFH** (Table S4).

Crystal structures of L-AcFH and *rac*-AcFH

We next examine in detail the structures of crystals grown in DMF, CH_3CN, and CH_3OH to elucidate the role of DMF. *rac*-**AcFH** crystallizes from DMF in the form of either L-**AcFH** or D-**AcFH**. In our analysis of the structure of crystals of L-**AcFH** grown in DMF, we identified a βII turn (for β-turn parameters, see Table S3) and found that one molecule of DMF interacts with two molecules of L-**AcFH** from two parallel helices along the *a* axis by hydrogen bonds using donor and acceptor from the same DMF molecule, N–H^b···O=CH-N(CH_3)-CH_2–H···S=C, and that one DMF molecule bridges the neighboring two helices separated by 10.87 Å (Figures 3A–3E and S3). This distance between two helices in the crystals of L-**AcFH** is much larger than that between two neighboring helices in the crystals of L-**AcAI** (7.81 Å),[12] likely due to the bulky benzyl substituent in phenylalanine residue in L-**AcFH**. The 3D superstructure of the crystal of L-**AcFH** shows that there are three supramolecular helices along the same *b* axis, which are, respectively, supported by the intermolecular (1) N–H^c···^{f}O=C and C=S···^{a}H–N hydrogen bonds in a supramolecular *M*-helix of pitch 7.60 Å (Figure 3A (for parameters and calculated energies of the hydrogen bonds, see Tables 1, S7, and S8), similar to the hydrogen-bonded *M*-helix in the crystals of L-**AcAH** and *rac*-**AcAH** (Table 1)[12]; (2) Ar–H^h···S=C hydrogen bonds between two adjacent phenylthiourea groups of L-**AcFH**, leading to a *P*-helix of pitch 7.60 Å (Figure 3B), which together with the first *M*-helix forms a homochiral

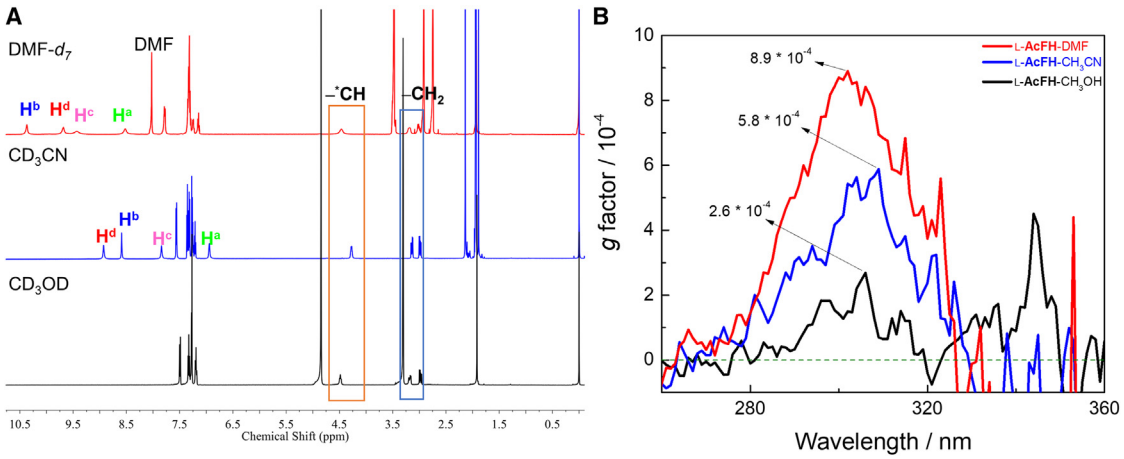

Figure 1. ^{1}H-NMR spectra and anisotropic factors

(A) ^{1}H-NMR spectra of L-**AcFH** in CD_3OD, CD_3CN, and DMF-d_7. [L-**AcFH**] = 2 mM.

(B) *g* factor profiles of L-**AcFH** crystals grown in CH_3OH, CH_3CN, and DMF.

layer within the *bc* plane (Figure 3D); and (3) Ar–$H^g\cdots{}^e$O=C hydrogen bonds resulting in an *M*-helix (Figure 3C), where the aromatic *meta*-C-H^g proton is from the phenylalanine residue, while the former *meta*-C-H^h proton is from the phenylthiourea moiety, both being newer binding sites than those in the alanine derivative L-**AcAl**.[12] The first and third *M*-helices (Figures 3A and 3C) form a homochiral layer within the *ab* plane (Figure 3E), which together with the homochiral layer within the *bc* plane ensures a 3D homochirality (Figure 3D). This represents a new interaction mode of forming three helices along the same axis that affords the 3D homochirality in the crystal and therefore accounts for the observed spontaneous resolution in DMF.

Crystals of L-**AcFH** grown in CH_3CN or CH_3OH also include solvent molecules via hydrogen bonding with L-**AcFH** (Figure S2). In the crystals grown in CH_3CN, there are two helices along the *b* axis, formed via interactions of (1) N–$H^c\cdots{}^f$O=C and C=S$\cdots{}^a$H–N hydrogen bonds (*M*-helicity, pitch 7.33 Å; Figure S4A; Tables 1, S7, and S8) and (2) the Ar–$H^h\cdots$S=C hydrogen bond between two adjacent phenylthiourea groups (*P*-helicity, pitch 7.33 Å; Figure S4B), creating a homochiral 2D layer within the *bc* plane (Figure S4C); both are the same as those observed in the crystals grown in DMF. The 2D layers further stack parallelly along the *a* axis via van der Waals interactions, between which solvent CH_3CN molecules are bonded by N–$H^b\cdots$N≡C hydrogen bonds using only the N atom in CH_3CN (Figures 4B and S4D). In the crystals grown in CH_3OH, two helices of *M*- and *P*-helicity of pitches (both 7.59 Å) were found along the *a* axis, which are formed via (1) N–$H^c\cdots{}^f$O=C and C=S$\cdots{}^a$H–N (Figure S4E) and (2) Ar–$H^h\cdots$S=C hydrogen bonds (Figure S4F), forming a homochiral 2D layer within the *ac* plane (Figure S4G), similar to that within the *bc* plane in the crystals grown in CH_3CN (Figure S4C). CH_3OH molecules participate in C=$O^e\cdots$H–O$\cdots{}^b$H–N double hydrogen bonds, using hydrogen-bonding donor and acceptor in its OH group, to bridge along the *b* axis those layers in an anti-parallel manner that leads to a 3D superstructure (Figures 4C and S4H). Note that in the crystals of L-**AcFH** grown in CH_3CN and CH_3OH, there are two helices along one axis that only one homochiral layer is formed, which is not sufficient to ensure the 3D homochirality required for spontaneous resolution. This is likely because of the unsuitable hydrogen-bonding mode of the solvent molecules with the helices. Only the solvent DMF molecule functions in that the distance between its hydrogen-bonding donor and acceptor is comparable to the size of the benzyl substituent in the phenylalanine residue in **AcFH**. In comparing the helices in L-**AcFH** crystals grown in DMF, CH_3CN, and CH_3OH, we conclude that the Ar–$H^g\cdots{}^e$O=C hydrogen-bonding interaction in DMF is an important factor (Table 1), which is absent in the crystals grown in CH_3CN and CH_3OH.

In the crystals of L-**AcFH** grown in DMF, CH_3CN, and CH_3OH, distances between the two main helices along the *c* axis that are each maintained by N–$H^c\cdots{}^f$O = C and C=S$\cdots{}^a$H–N hydrogen bonds, are, respectively, 13.54, 13.54, and 13.25 Å (Figures 3D and S5). Those distances are much larger than those in the crystals of the L-**AcAH** crystal (7.81 Å; Figure S5)[12]—they are themselves close to one another. This means that this large distance results from the bulky benzyl substituent in the phenylalanine residue, which may explain the absence in the crystals of L-**AcFH** of the inter-helix N–$H^b\cdots{}^e$O=C hydrogen bonds that were observed in the crystal of L-**AcAH,** with a much smaller substituent, –CH_3, in its alanine residue.[12] However, a new hydrogen bond of Ar–$H^h\cdots$S=C in the crystal of L-**AcFH** may have served to release the steric hindrance (Figure S5) and to support the *P*-helix (Figures 2, 3, and S4). Calculations using crystal structure parameters show that the strength of the intramolecular 10-membered ring hydrogen bond that maintains the β-turn in L-**AcFH** follows the order of crystals grown in DMF > CH_3CN > CH_3OH—the same as that of the hydrogen bond length (Table S3) and of the maximum dissymmetric *g* factors of the crystals of L-**AcFH** (Figure 1B). Therefore, L-**AcFH** crystals grown in DMF show a more stable β-turn structure and stronger supramolecular helicity than those crystals grown in CH_3CN and CH_3OH. The structure of the crystals of D-**AcFH** is a mirror image of that of L-**AcFH** (Figures S6 and S7; Table S2).

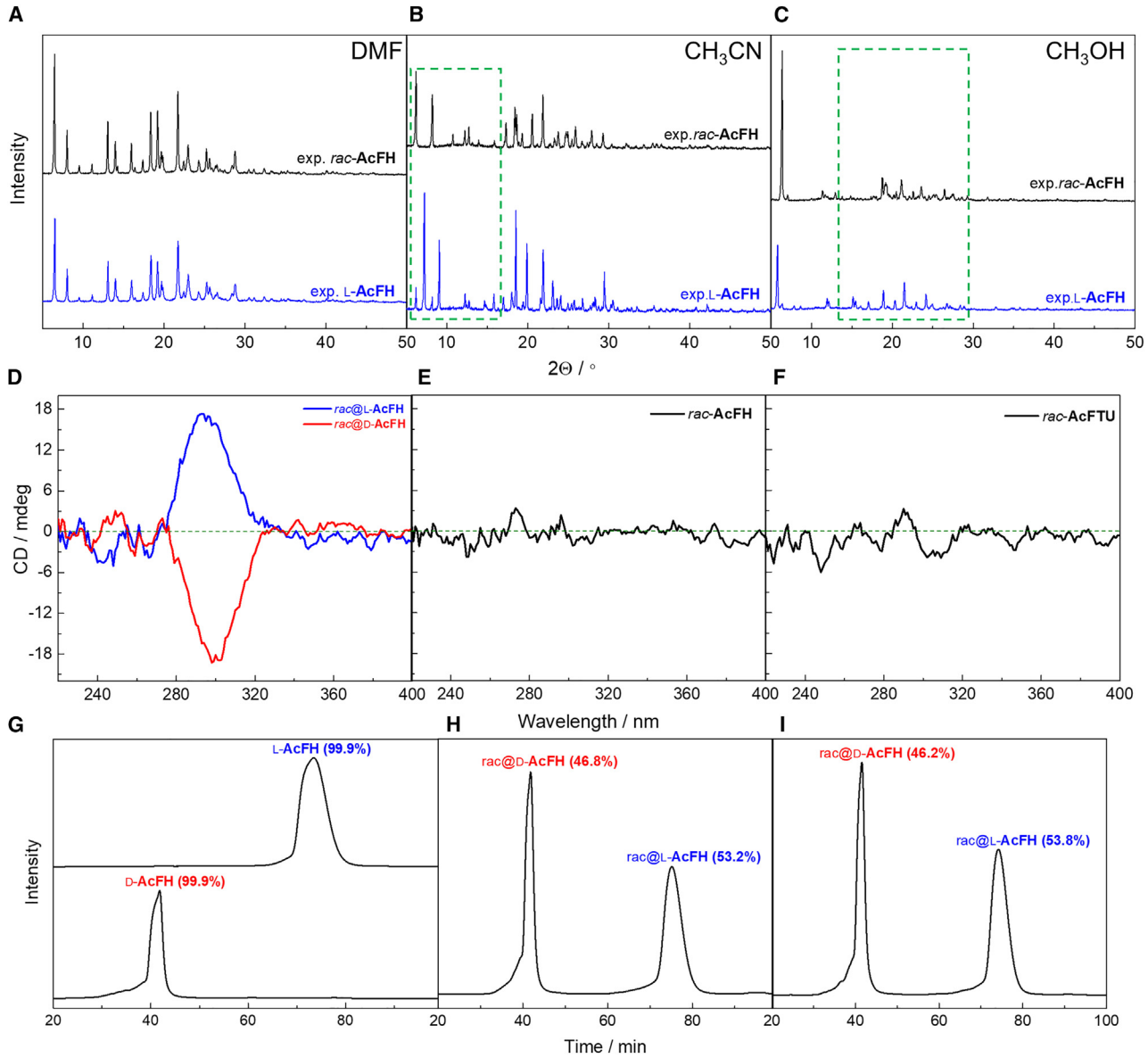

Figure 2. XRPD patterns, solid-state CD spectra, and HPLC traces

(A–C) XRPD patterns of crystals of L-**AcFH** and *rac*-**AcFH** grown in DMF (A), CH_3CN (B), or CH_3OH (C).

(D–F) Solid-state CD spectra of single crystal of *rac*-**AcFH** grown in DMF (D), CH_3CN (E), or CH_3OH (F).

(G–I) HPLC traces of selected single crystals of *rac*-**AcFH** grown in DMF (G), CH_3CN (H), or CH_3OH (I). For HPLC, column: Chiralpak@ID (250 × 4.6 mm); mobile phase: 47:53 (v/v) *n*-hexane/2-propanol; flow rate: 1.0 mL/min; UV detection wavelength: 270 nm.

A racemic crystallization of *rac*-**AcFH** in CH_3CN and CH_3OH was thus expected to take place (Table S6). Crystals grown from *rac*-**AcFH** in CH_3CN show an achiral $P2_1/c$ space group, containing equal equivalents of L-**AcFH** and D-**AcFH** (labeled, respectively, as *rac*@L-**AcFH** and *rac*@D-**AcFH**). In the crystal of *rac*@L-**AcFH**, an *M*-helix supported by hydrogen bonds N–$H^{c}\cdots{}^{f}$O=C and N–$H^{a}\cdots$S=C and a *P*-helix by Ar–$H^{h}\cdots$S=C hydrogen bonds, both along the *b* axis, were found (Figures S8A and S8B), forming a homochiral 2D layer within the *ab* plane (Figure S8C), which is the same as that seen in the crystals of enantiopure L-**AcFH** (Figures S4A and S4B). However, the homochiral 2D layers formed from *rac*@L-**AcFH** and *rac*@D-**AcFH** stack alternatively along the *c* axis in a parallel manner, resulting in a racemic 3D superstructure (Figure S8D). Between those alternative layers, double Ar–$H^{g}\cdots\pi$ interactions take place (Figure 4D), while solvent CH_3CN molecules are anchored via the N–$H^{b}\cdots$N≡C hydrogen bonds between two molecules of **AcFH** of opposite chirality (Figure 4D).

In the crystals grown from *rac*-**AcFH** in CH_3OH, only one helix along the *b* axis was found holding molecules via N–$H^{c}\cdots{}^{f}$O=C/N–$H^{a}\cdots$S=C hydrogen bonds (Figure S8E). CH_3OH molecules take part in the N–$H^{b}\cdots$H–O$\cdots{}^{e}$O=C hydrogen bonds bridging

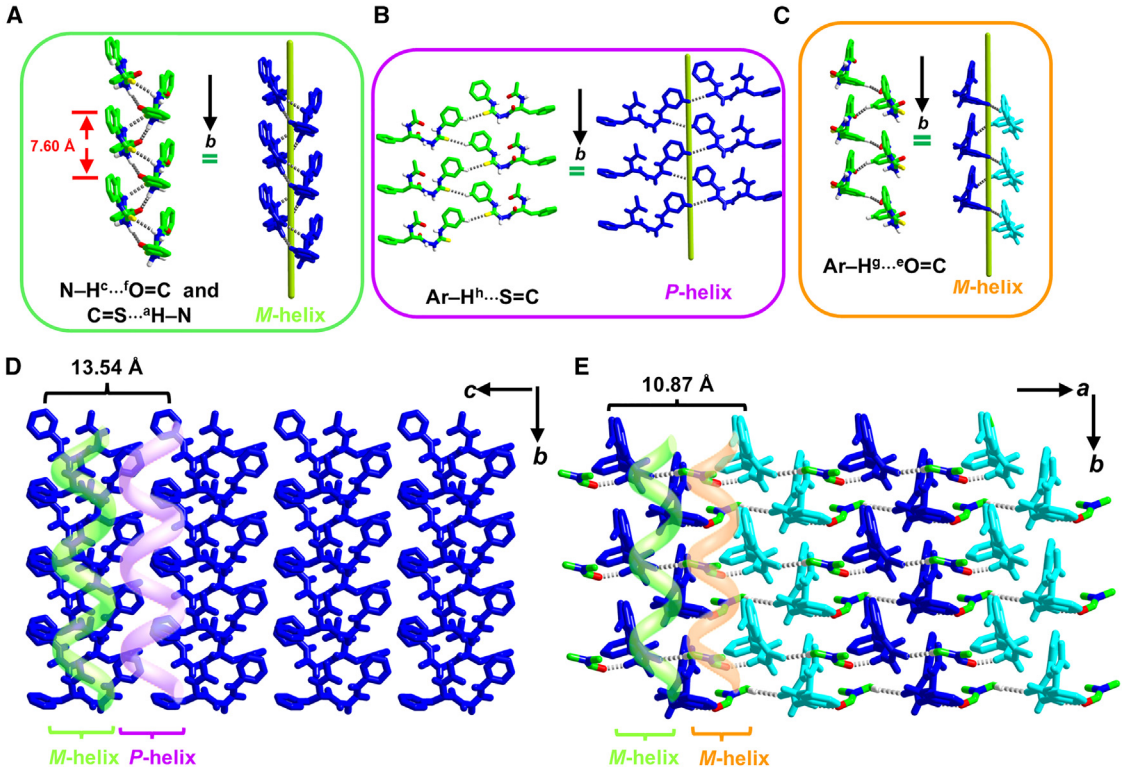

Figure 3. X-ray structures of L-AcFH grown in DMF

(A) N–H^{c}···^{f}O=C/C=S··· ^{a}H–N hydrogen bonds (dashed gray lines) maintain an *M*-helix along the *b* axis.

(B) Ar–H^{h}···S=C hydrogen bonds (dashed gray lines) maintain a *P*-helix along the *b* axis.

(C) Ar–H^{g}···^{e}O=C hydrogen bonds (dashed gray lines) maintain an *M*-helix along the *b* axis.

(D) A 2D homochiral superstructure within the *bc* plane.

(E) A 2D homochiral superstructure within the *ab* plane, in which DMF solvent molecules bridge, via hydrogen bonds, the neighboring two helices, further stabilizing the 2D structure.

two heterochiral 1D helices along the *a* axis in an anti-parallel manner (Figure 4E), while van der Waals interactions take place along the *c* axis in a parallel manner, resulting in a racemic 3D superstructure of only 1D homochirality (Figure S8F). Calculated energy based on the structure of crystal of *rac*@L-**AcFH** grown in CH_3OH is lower than that of L-**AcFH** by a high value of 37.70 kJ mol^{-1} (Figure S9), explaining the racemic crystallization of *rac*-**AcFH** in CH_3OH. In both cases of crystallization of *rac*-**AcFH** in CH_3CN and CH_3OH, the solvent molecule bridges two building-block molecules of opposite chirality, probably due to the smaller size of these hydrogen-bonding solvents that make the heterochiral L-/D-phenylalanine $\pi\cdots\pi$ interactions[25] more prominent, again highlighting the critical role of the bulky solvent DMF.

Spontaneous resolution of AcFI in DMF

To strengthen this conclusion, we crystallized racemic **AcFI** (Scheme 1), a phenylalanine counterpart of **AcAI** containing the halogen bonding I atom[12] in DMF. Spontaneous resolution was found to occur, but now with DMF molecules included within the lattice (Figures S10–S13; Table S9). Three supramolecular helices along three axes were found (Figure S12), two of which are similar to those previously found in the crystal of L- or D-**AcAI**,[12] while the third one (Ar–H^{g}···^{e}O=C hydrogen-bonded helix) is the same as that observed in the crystals of **AcFH** grown in DMF (Table 1). These three helices along three axes in **AcFI** differ from the three helices along the same axis in the crystals of **AcFH** grown in the same solvent DMF, highlighting the inevitable contributions of the halogen bonding between **AcFI** molecules and the participation of DMF solvent molecules in the spontaneous resolution of **AcFX** (X = H, I). Very interestingly, despite the structural characters of the intermolecular hydrogen and halogen bonding in **AcFI** that are similar to those in **AcAI**,[12] spontaneous resolution of **AcFI** does not occur in solvents such as CH_3OH and CH_3CN (Figure S14; Table S10), in which **AcAI** underwent spontaneous solution.[12] Again, this highlights the critical role of DMF for spontaneous resolution of the helical building block bearing a bulky amino acid residue that would enlarge the distance between the formed neighboring two helices.

Examining structural data summarized in Table 1, we found that in the current helical structural motif of *N*-amido-*N*′-phenylthiourea containing a β-turn starting from an acetyl amino acid (Scheme 1), hydrogen bonds N–H^{c}···^{f}O=C and N–H^{a}···S=C that lead to an *M*-helix in case of L-amino acid derivative are a common interaction mode. With the *para*-halogen-substituted *N*′-phenyl derivatives, halogen bonding involving C–I leads to an *M*-helix. Specific

Table 1. Crystal system, space group, and parameters of supramolecular helices of L-AcFH and L-AcFI in their enantiopure and racemic crystals

Crystal system	Space group	Sense	Helical pitch, Å	Hydrogen bonds
L-AcFH (DMF)				
monoclinic	$P2_1$	*M*	7.60	N–H^{c}···^{f}O=C ($d_{H\cdots O}$ = 2.076 Å; ∠NHO = 141.8°) N–H^{a}···S=C ($d_{H\cdots S}$ = 2.639 Å; ∠NHS = 140.6°)
		P	7.60	Ar–H^{h}···S=C ($d_{H\cdots S}$ = 2.908 Å; ∠CHS = 150.2°)
		M	7.60	Ar–H^{g}···^{e}O=C ($d_{H\cdots O}$ = 2.528 Å; ∠CHO = 135.8°)
L-AcFH (CH_3CN)				
monoclinic	$P2_1$	*M*	7.33	N–H^{c}···^{f}O=C ($d_{H\cdots O}$ = 2.069 Å; ∠NHO = 137.1°) N–H^{a}···S=C ($d_{H\cdots S}$ = 2.682 Å; ∠NHS = 143.1°)
		P	7.33	Ar–H^{h}···S=C ($d_{H\cdots S}$ = 2.868 Å; ∠CHS = 142.1°)
rac@L-AcFH (CH_3CN)				
monoclinic	$P2_1/c$	*M*	7.35	N–H^{c}···^{f}O=C ($d_{H\cdots O}$ = 2.094 Å; ∠NHO = 136.2°) N–H^{a}···S=C ($d_{H\cdots S}$ = 2.674 Å; ∠NHS = 142.2°)
		P	7.35	Ar–H^{h}···S=C ($d_{H\cdots S}$ = 2.867 Å; ∠CHS = 143.0°)
L-AcFH (CH_3OH)				
orthorhombic	$P2_12_12$	*M*	7.59	N–H^{c}···^{f}O=C ($d_{H\cdots O}$ = 2.114 Å; ∠NHO = 140.5°) N–H^{a}···S=C ($d_{H\cdots S}$ = 2.604 Å; ∠NHS = 142.9°)
		P	7.59	Ar–H^{h}···S=C ($d_{H\cdots S}$ = 2.798 Å; ∠CHS = 144.1°)
rac@L-AcFH (CH_3OH)				
orthorhombic	Pbca	*M*	7.71	N–H^{c}···^{f}O=C ($d_{H\cdots O}$ = 2.080 Å; ∠NHO = 144.0°) N–H^{a}···S=C ($d_{H\cdots S}$ = 2.594 Å; ∠NHS = 145.9°)
L-AcFI (DMF)				
orthorhombic	$P2_12_12_1$	*M*	7.99	N–H^{c}···^{f}O=C ($d_{H\cdots O}$ = 2.052 Å; ∠NHO = 147.9°) N–H^{a}···S=C ($d_{H\cdots S}$ = 2.600 Å; ∠NHS = 140.3°)
		P	16.49	Ar–H^{g}···^{e}O=C ($d_{H\cdots O}$ = 2.587 Å; ∠CHO = 164.9°)
		M	18.13	C–I···π ($d_{I\cdots\pi}$ = 4.095 Å; ∠CIπ = 153.9°)
L-AcAH[12]				
orthorhombic	$P2_12_12_1$	*M*	7.66	N–H^{c}···^{f}O=C ($d_{H\cdots O}$ = 2.137 Å; ∠NHO = 141.9°) N–H^{a}···S=C ($d_{H\cdots S}$ = 2.729 Å; ∠NHS = 145.4°)
L-AcAI[12]				
orthorhombic	$P2_12_12_1$	*M*	7.90	N–H^{c}···^{f}O=C ($d_{H\cdots O}$ = 2.104 Å; ∠NHO = 143.4°) N–H^{a}···S=C ($d_{H\cdots S}$ = 2.695 Å; ∠NHS = 144.6°)
		M	7.86	C–I···S=C ($d_{I\cdots S}$ = 3.488 Å; ∠CIS = 172.5°)

For comparison, the crystal system, space group, and parameters of supramolecular helices of L-**AcAH** and L-**AcAI** are listed.

to the derivatives of **AcFX** (X = H and I) reported here, Ar–H^{g}···^{e}O=C hydrogen bonding is shown to commonly lead to a helix via interaction involving the phenyl *meta*-C–H proton from the phenylalanine residue.

Notably, **AcFH** remained to crystallize as racemic compounds in CH_3OH and CH_3CN in cases in which chiral L-**AcFH** crystal seeds were introduced[10] or slow evaporation was performed at lowered temperature of 4°C. This also holds when an **AcFH** of 20% *ee* was allowed to crystallize. Our ongoing research includes the addition of chiral additives[5,8] and modifications in pressure[30] to explore whether spontaneous resolution could occur in CH_3OH and CH_3CN.

DISCUSSION

We achieved the spontaneous resolution of the amino acid phenylalanine, which bears the bulky substituent benzyl, by crystallizing the helical derivatives **AcFH** and **AcFI** in DMF and 1:1:1 (v/v/v) DMF/CH_3CN/CH_3OH. In both cases, DMF molecules, but not the other solvents, were included within the crystal lattices. We are therefore able to show the critical role of solvent DMF for the spontaneous resolution. This bulky and hydrogen-bonding solvent molecule contains both a hydrogen-bonding donor and an acceptor, separated by a distance comparable to the size of the bulky substituent in the amino acid residue, bridging the two neighboring helices of the building block via of N–H^{b}···O=CH-N(CH_3)-CH_2–H···S=C hydrogen bonds. In solvents of similar structural characters but of smaller sizes, such as CH_3OH and CH_3CN, spontaneous resolution does not take place. Future efforts should be made to discover new spontaneous resolution systems to help better understand how the nature of the substituent in amino acid residues would define the choice of solvents.

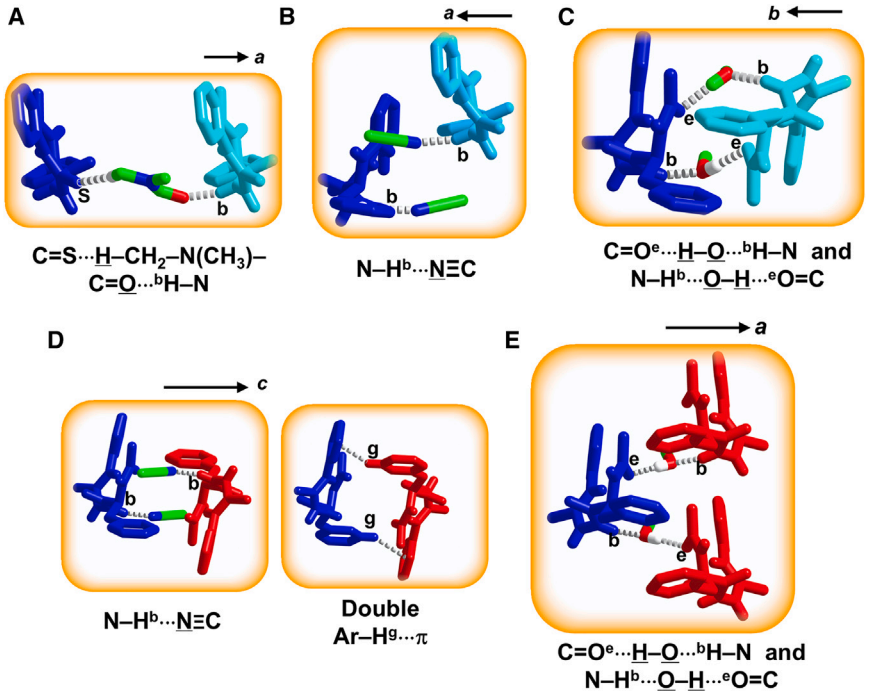

Figure 4. Structures showing hydrogen bonding of solvent molecules, with L-AcFH crystals grown in DMF, CH_3CN, and CH_3OH and *rac*-AcFH crystals grown in CH_3CN (D) and CH_3OH (E)

(A) C=S···H–C and C=O···^{b}H–N hydrogen bonds along the *a* axis between one DMF molecule and two L-**AcFH** molecules from two neighboring helices.

(B) N–H^{b}···N≡C hydrogen bonds between L-**AcFH** and CH_3CN molecule.

(C) Double C=O^{e}···H–O···^{b}H–N hydrogen bonds between L-**AcFH** and CH_3OH molecule along the *b* axis.

(D) N–H^{b}···N≡C hydrogen bonds (dashed light gray lines) between **AcFH** and CH_3CN molecules, and double Ar–H^{g}···π hydrogen bonds (dashed light gray lines) between heterochiral molecules along the *c* axis.

(E) CH_3OH solvent molecules take part in N–H^{b}···O–H···^{e}O=C hydrogen bonds to bridge two heterochiral molecules along the *a* axis. For clarity, –CH protons except those forming intermolecular hydrogen bonds are omitted.

Note that in (D) and (E), L-**AcFH** is shown in blue and D-**AcFH** is shown in red.

METHODS

Additional details regarding the methods can be found in the supplemental information.

Synthesis of D-AcFH and L-/D-AcFI

L-**AcFH** was synthesized and characterized according to our previous procedures.[27]

1. D-**AcFOEt**: 2.30 g (10.0 mmol) D-**H-FOEt·HCl** was added to 20 mL $CHCl_3$, and 1.5 mL Et_3N was added at ambient temperatures dropwise to make the solution clear and transparent. The solution was then added to a 10-mL $CHCl_3$ solution containing 1.5 mL CH_3COCl. The mixture was stirred at room temperature for 4 h. Solvent was removed by evaporation *in vacuo*, followed by the addition of 20 mL ethyl acetate and 20 mL pure water. The organic phase was washed with diluted $NH_3 \cdot H_2O$ (0.1 M), diluted HCl (0.1 M), and saturated NaCl solution several times in turn, and was dried by anhydrous Na_2SO_4. Solvent was removed by evaporation *in vacuo* to afford a colorless oil, D-**AcFOEt**.
2. D-**AcFN$_2$H$_3$**: Excess aqueous hydrazine (85%, 4.0 mL) was added to D-**AcFOEt** in EtOH (30 mL), and the mixture was refluxed for 12 h. Solvent was removed by evaporation *in vacuo*, and the crude product was washed with EtOH and Et_2O to afford white solid D-**AcFN$_2$H$_3$**.
3. D-**AcFH**: D-**AcFN$_2$H$_3$** (0.22 g, 1.0 mmol) was added to excess (1.5 mmol) phenyl isothiocyanate dissolved in 30 mL CH_3CN, and the solution was refluxed for 24 h. Solvent was removed by evaporation *in vacuo*, and the crude product was washed with Et_2O several times to afford pure white solid D-**AcFH** (0.21 g, 60% yield).
4. L-/D-**AcFI**: L-/D-**AcFN$_2$H$_3$** (0.22 g, 1.0 mmol) was added to excess phenyl isothiocyanate (0.32 g, 1.2 mmol) in 30 mL CH_3CN, and the solution was refluxed for 24 h. Solvent was removed by evaporation *in vacuo*, and the crude product was washed with CH_3CN and Et_2O several times to afford pure white solid L-/D-**AcFI** (0.22 g, 46% yield).

RESOURCE AVAILABILITY

Lead contact

Further information and requests for resources should be directed to and will be fulfilled by the lead contact, Yun-Bao Jiang (ybjiang@xmu.edu.cn).

Materials availability

This study did not generate new unique materials.

Data and code availability

- Data: Single crystallographic data have been deposited at the Cambridge Crystallographic Data Center (CCDC) as deposition number CCDC 2211530, 2211531, 2211532, 2211533, 2211534, 2311162, 2311163, 2386124, 2386125, and 2386126 and are publicly available as of the date of publication. The deposition number contains the supplementary crystallographic data for this paper. These data are provided free of charge by the joint CCDC and Fachinformationszentrum Karlsruhe Access Structures service.
- Code: All data generated or analyzed during this study are included in the published article and its supplemental information.
- All other raw data and code used for analysis not included in the supplemental information are available from the lead contact upon reasonable request.

ACKNOWLEDGMENTS

We are grateful for the support of this work by the National Science Foundation of China (grant nos. 21820102006, 22101240, 22241503, and 92356308), the Fundamental Research Funds for the Central Universities (grant nos.

20720220005 and 20720220121), and the Fujian Provincial Natural Science Foundation of China (grant no. 2023J01038).

AUTHOR CONTRIBUTIONS

X.Y. and Y.-B.J. conceived the study. P.W. performed the majority of the experiments, with contributions from X.L., Y.-L.C., J.C., and Z.L. P.W. wrote the first draft, with suggestions from the other authors. Y.-B.J. revised the draft.

DECLARATION OF INTERESTS

The authors declare no competing interests.

SUPPLEMENTAL INFORMATION

Supplemental information can be found online at https://doi.org/10.1016/j.xcrp.2025.102521.

Received: October 31, 2024
Revised: December 14, 2024
Accepted: March 11, 2025
Published: April 7, 2025

REFERENCES

1. Brock, C.P., and Dunitz, J.D. (1994). Towards a Grammar of Crystal Packing. Chem. Mater. *6*, 1118–1127. https://doi.org/10.1021/cm00044a010.
2. Pérez-García, L., and Amabilino, D.B. (2002). Spontaneous resolution under supramolecular control. Chem. Soc. Rev. *31*, 342–356. https://doi.org/10.1039/b201099m.
3. Pérez-García, L., and Amabilino, D.B. (2007). Spontaneous resolution, whence and whither: from enantiomorphic solids to chiral liquid crystals, monolayers and macro- and supra-molecular polymers and assemblies. Chem. Soc. Rev. *36*, 941–967. https://doi.org/10.1039/b610714a.
4. Noorduin, W.L., Vlieg, E., Kellogg, R.M., and Kaptein, B. (2009). From Ostwald ripening to single chirality. Angew. Chem. Int. Ed. *48*, 9600–9606. https://doi.org/10.1002/anie.200905215.
5. Lazarou, K.A., González-Nieves, K., Chakraborty, I., and Raptis, R.G. (2019). Spontaneous resolution by crystallization of an octanuclear Iron(III) complex using only racemic reagents. Angew. Chem. Int. Ed. *58*, 7324–7328. https://doi.org/10.1002/anie.201901877.
6. Wehner, M., Röhr, M.I.S., Stepanenko, V., and Würthner, F. (2020). Control of self-assembly pathways toward conglomerate and racemic supramolecular polymers. Nat. Commun. *11*, 5460. https://doi.org/10.1038/s41467-020-19189-8.
7. Buhse, T., Cruz, J.M., Noble-Terán, M.E., Hochberg, D., Ribó, J.M., Crusats, J., and Micheau, J.C. (2021). Spontaneous Deracemizations. Chem. Rev. *121*, 2147–2229. https://doi.org/10.1021/acs.chemrev.0c00819.
8. Uno, M., Kojima, T., Kuwamura, N., Yoshinari, N., and Konno, T. (2021). Racemic Tartrate/Malate Anions Combine with Racemic Complex Cations to Form Optically Active Ionic Crystals. Chem. Eur J. *27*, 8358–8364. https://doi.org/10.1002/chem.202100576.
9. Putman, J.I., and Armstrong, D.W. (2022). Recent advances in the field of chiral crystallization. Chirality *34*, 1338–1354. https://doi.org/10.1002/chir.23492.
10. Borchardt-Setter, K.A., Yu, J., Yao, X., Shen, Y., Guzei, I., and Yu, L. (2024). Chiral Resolution by Seeded Crystallization: The Case of Arabitol. Cryst. Growth Des. *24*, 9053–9058. https://doi.org/10.1021/acs.cgd.4c01072.
11. Weng, P., Yan, X., and Jiang, Y.-B. (2023). Formation of Multiple Supramolecular Helices for Spontaneous Resolution. ChemSystemsChem *5*, e202200043. https://doi.org/10.1002/syst.202200043.
12. Lin, X., Kou, B., Cao, J., Weng, P., Yan, X., Li, Z., and Jiang, Y.-B. (2022). Spontaneous resolution of helical building blocks through the formation of homochiral helices in two dimensions. Angew. Chem. Int. Ed. *61*, e202205914. https://doi.org/10.1002/anie.202205914.
13. Yan, X., Weng, P., Cao, J., Lin, K., Qi, Y., Wu, X., and Jiang, Y.-B. (2024). Simultaneous formation of helical and sheet-like assemblies from short azapeptides enables spontaneous resolution. Nanoscale *16*, 19221–19227. https://doi.org/10.1039/d4nr02872d.
14. Wang, J., Liu, K., Yan, L., Wang, A., Bai, S., and Yan, X. (2016). Trace solvent as a predominant factor to tune dipeptide self-assembly. ACS Nano *10*, 2138–2143. https://doi.org/10.1021/acsnano.5b06567.
15. Xing, P., Yang, C., Wang, Y., Phua, S.Z.F., and Zhao, Y. (2018). Solvent-Controlled Assembly of Aromatic Glutamic Dendrimers for Efficient Luminescent Color Conversion. Adv. Funct. Mater. *28*, 1802859. https://doi.org/10.1002/adfm.201802859.
16. Xue, S., Xing, P., Zhang, J., Zeng, Y., and Zhao, Y. (2019). Diverse Role of Solvents in Controlling Supramolecular Chirality. Chem. Eur J. *25*, 7426–7437. https://doi.org/10.1002/chem.201900714.
17. Mabesoone, M.F.J., Palmans, A.R.A., and Meijer, E.W. (2020). Solute-Solvent Interactions in Modern Physical Organic Chemistry: Supramolecular Polymers as a Muse. J. Am. Chem. Soc. *142*, 19781–19798. https://doi.org/10.1021/jacs.0c09293.
18. Shemchuk, O., Spoletti, E., Braga, D., and Grepioni, F. (2021). Solvent Effect on the Preparation of Ionic Cocrystals of dl-Amino Acids with Lithium Chloride: Conglomerate versus Racemate Formation. Cryst. Growth Des. *21*, 3438–3448. https://doi.org/10.1021/acs.cgd.1c00216.
19. Tunyogi, T., Deák, A., Tárkányi, G., Király, P., and Pálinkás, G. (2008). Solvent-assisted spontaneous resolution of a 16-membered ring containing gold(I) showing short Au···Au aurophilic interaction and a figure-eight conformation. Inorg. Chem. *47*, 2049–2055. https://doi.org/10.1021/ic702059v.
20. Cucinotta, A., Kahlfuss, C., Minoia, A., Eyley, S., Zwaenepoel, K., Velpula, G., Thielemans, W., Lazzaroni, R., Bulach, V., Hosseini, M.W., et al. (2023). Metal ion and guest-mediated spontaneous resolution and solvent-induced chiral symmetry breaking in guanine-based metallosupramolecular networks. J. Am. Chem. Soc. *145*, 1194–1205. https://doi.org/10.1021/jacs.2c10933.
21. Walther, A., Tusha, G., Schmidt, B., Holstein, J.J., Schäfer, L.V., and Clever, G.H. (2024). Solvent-Directed Social Chiral Self-Sorting in Pd_2L_4 Coordination Cages. J. Am. Chem. Soc. *146*, 32748–32756. https://doi.org/10.1021/jacs.4c12525.
22. Zhang, J., Zhao, Z., Zhang, J., She, S., Huang, Y., and Wei, Y. (2014). Spontaneous resolution of polyoxometalate-based inorganic–organic hybrids driven by solvent and common ion. Dalton Trans. *43*, 17296–17302. https://doi.org/10.1039/c4dt01954g.
23. Sarmah, K.K., Rajbongshi, T., Bhuyan, A., and Thakuria, R. (2019). Effect of solvent polarity in mechanochemistry: preparation of a conglomerate vs. racemate. Chem. Commun. *55*, 10900–10903. https://doi.org/10.1039/c9cc05687d.
24. Li, X.Z., Li, M., Li, Z., Hou, J.Z., Huang, X.C., and Li, D. (2008). Concomitant and controllable chiral/racemic polymorphs: from achirality to isotactic, syndiotactic, and heterotactic chirality. Angew. Chem. Int. Ed. *47*, 6371–6374. https://doi.org/10.1002/anie.200801481.
25. Zong, Z., Li, P., Hao, A., and Xing, P. (2020). Self-assembly of *N*-terminal aryl amino acids into adaptive single- and double-strand helices. J. Phys. Chem. Lett. *11*, 4147–4155. https://doi.org/10.1021/acs.jpclett.0c00997.
26. Yan, X.S., Wu, K., Yuan, Y., Zhan, Y., Wang, J.H., Li, Z., and Jiang, Y.-B. (2013). β-Turn structure in glycinylphenylalanine dipeptide based *N*-amidothioureas. Chem. Commun. *49*, 8943–8945. https://doi.org/10.1039/c3cc44336a.

27. Yan, X.-S., Luo, H., Zou, K.-S., Cao, J.-L., Li, Z., and Jiang, Y.-B. (2018). Short Azapeptides of Folded Structures in Aqueous Solutions. ACS Omega *3*, 4786–4790. https://doi.org/10.1021/acsomega.8b00041.

28. Cao, J., Yan, X., He, W., Li, X., Li, Z., Mo, Y., Liu, M., and Jiang, Y.-B. (2017). C–I···π Halogen Bonding Driven Supramolecular Helix of Bilateral *N*-Amidothioureas Bearing β-Turns. J. Am. Chem. Soc. *139*, 6605–6610. https://doi.org/10.1021/jacs.6b13171.

29. Yan, X., Zou, K., Cao, J., Li, X., Zhao, Z., Li, Z., Wu, A., Liang, W., Mo, Y., and Jiang, Y. (2019). Single-handed supramolecular double helix of homochiral bis(*N*-amidothiourea) supported by double crossed C-I···S halogen bonds. Nat. Commun. *10*, 3610. https://doi.org/10.1038/s41467-019-11539-5.

30. Roszak, K., and Katrusiak, A. (2018). High-pressure and temperature dependence of the spontaneous resolution of 1,1′-binaphthyl enantiomers. Phys. Chem. Chem. Phys. *20*, 5305–5311. https://doi.org/10.1039/c7cp07234a.